RW Doradus: A solar-type shallow contact binary with a new orbital period investigation

Thawicharat Sarotsakulchai (ID),[1,2,3,*] **Sheng-Bang** Qian,[1,2,4,5]
Boonrucksar Soonthornthum,[3] **Eduardo** Fernández Lajús,[6,7]
Nian-Ping Liu,[1,4,5] **Xiao** Zhou,[1,4,5] **Jia** Zhang,[1,4,5] **Wen-Ping** Liao,[1,4,5]
Daniel E. Reichart,[8] **Joshua B.** Haislip,[8] **Vladimir V.** Kouprianov,[8]
and Saran Poshyachinda[3]

[1]Yunnan Observatories, Chinese Academy of Sciences, 650216 Kunming, China
[2]University of Chinese Academy of Sciences, 19A Yuquan Road, Shijingshan, 100049 Beijing, China
[3]National Astronomical Research Institute of Thailand, Ministry of Science and Technology, Bangkok, Thailand
[4]Key Laboratory of the Structure and Evolution of Celestial Objects, Chinese Academy of Sciences, 650216 Kunming, China
[5]Center for Astronomical Mega-Science, Chinese Academy of Sciences, 20A Datun Road, Chaoyang District, Beijing, 100012, China
[6]Facultad de Ciencias Astronómicas y Geofísicas – UNLP, 1900 La Plata, Buenos Aires, Argentina
[7]Instituto de Astrofísica de La Plata – CONICET/UNLP, 1900 La Plata, Buenos Aires, Argentina
[8]Department of Physics and Astronomy, University of North Carolina, CB #3255, Chapel Hill, NC 27599, USA

*E-mail: tavijarus@narit.or.th

Abstract

New CCD photometric light curves of the short-period ($P = 0.285$ d) eclipsing binary RW Dor are presented. The observations were performed with the PROMPT-8 robotic telescope at CTIO in Chile between 2015 March and 2017 March. Other eclipse timings were obtained from the 2.15 m JS telescope at CASLEO, San Juan, Argentina in 2011 December. Based on a light curve analysis, it is found that RW Dor is a W-type shallow contact binary with a fill-out factor $f \sim 11\%$ and a high mass ratio $q \sim 1.587$ ($1/q = 0.63$), where the hotter component is the less massive one ($M_1 \sim 0.52\,M_\odot$ and $M_2 \sim 0.82\,M_\odot$). For orbital-period investigation, 15 new eclipse times and those previously published were compiled. $O - C$ analysis with very weak evidence suggests that a long-term decrease in period with a rate of $dP/dt = -9.61 \times 10^{-9}$ d yr^{-1} is superimposed on a cyclic variation ($A_3 = 0.0054$ d and $P_3 = 49.9$ yr). The long-term decrease can be interpreted as mass transfer from the more massive component to the less massive one, or combined with angular momentum loss via magnetic braking. In addition, the marginal contact phase, high mass ratio ($1/q > 0.4$), and long-term decrease in period all suggest that RW Dor is a newly formed contact binary via Case A mass transfer, and it will evolve into a deeper normal contact binary. If the cyclic change is correct, the light travel-time effect via the presence of a cool third body will be a more plausible explanation for this.

1 Introduction

RW Dor (HD 269320, HIP 24763) is an important binary for studying the formation and evolution of a newly formed contact binary after the common convective envelope has been formed and in the transition either from detached or semi-detached into the contact phase, because there are few contact binaries that have been found to be newly formed or at the beginning of the contact phase that will evolve into normal contact binary stars when their mass ratio becomes higher, e.g., RV Psc (He & Qian 2009) and V524 Mon (He et al. 2012). RW Dor is a short-period W UMa-type binary with an orbital period of 0.285 d that is very close to a new period distribution of EW-type contact binaries with a peak of 0.29 d published by Qian et al. (2017b), indicating that RW Dor is a typical W UMa-type contact binary that is in agreement with the report (Qian et al. 2017a). The system is near the Large Magellanic Cloud (LMC), but is not a member of the LMC as pointed out by Russo, Vittone, and Milano (1984) and Marino et al. (2007). RW Dor was discovered as a variable star by Leavitt (1908), and later classified as a W UMa-type eclipsing binary by Hertzsprung (1925). The first spectral classification of the variable was made by Cannon (1921), who gave a spectral type of K5. This was subsequently confirmed by McLaughlin (1927), who also classified the system as a late-type eclipsing binary with the same spectral type.

The first photographic times of light minima were reported by Hertzsprung (1928), who gave an orbital period of 0.143 d. Later, eclipse times were obtained by many authors (e.g., Russo et al. 1984; Marton et al. 1989; Kaluzny & Caillault 1989; Ogloza & Zakrzewski 2004; Marino et al. 2007) and the linear ephemeris of the binary was also corrected. The complete light curves were analyzed with the Wilson–Devinney method (Wilson & Devinney 1971) by Marton, Grieco, and Sistero (1989) and Kaluzny and Caillault (1989), who determined the photometric elements independently. Those solutions indicated that RW Dor belongs to a W-subtype contact binary with components not in poor thermal contact, as predicted by the thermal relaxation oscillation theory (Lucy & Wilson 1979). Additionally, it was found that the light curves of RW Dor exhibited a significant difference in the depths of the minima and showed variation. Marton, Grieco, and Sistero (1989) explained the asymmetry in the light curves as a hot spot on the cooler and more massive component located near the neck connecting the stars, while Kaluzny and Caillault (1989) reported that their light curves were only marginally asymmetric and did not show any scatter beyond the observational errors.

The first radial velocity measurements of RW Dor were published by Hilditch, Hill, and Bell (1992) using the 3.9 m telescope of the Anglo-Australian Observatory. They found that RW Dor was composed of two K1-type stars and determined a spectroscopic mass ratio of $q_{sp} = 0.68$. By combining the photometric solutions given by Kaluzny and Caillault (1989), Hilditch, Hill, and Bell (1992) derived the absolute parameters of the binary system. They confirmed that RW Dor is a W-subtype contact binary. Other radial velocity V_0 curves were obtained by Duerbeck and Rucinski (2007), who determined a spectroscopic mass ratio of $q_{sp} = 0.63$, which is close to that derived by Hilditch, Hill, and Bell (1992). However, they found $V_0 = 25 \, \mathrm{km \, s^{-1}}$, which is somewhat smaller than the $V_0 = 66.5 \, \mathrm{km \, s^{-1}}$ given by Hilditch, Hill, and Bell (1992). Marino et al. (2007) reported that some light curves of RW Dor exhibited asymmetry, being similar to the results published by Marton, Grieco, and Sistero (1989). They also recomputed the spectroscopic mass ratio by using the radial velocities given by Hilditch, Hill, and Bell (1992) and Duerbeck and Rucinski (2007). All the eclipse times were also reanalyzed, and they found a secular decrease in orbital period with a rate of $\Delta P / P \sim -6.3 \times 10^{-11}$. However, neither light curve variation nor the third light in the system have been found in recent publications (e.g., Deb & Singh 2011).

In this paper we examine the variations of the light curve and determine new photometric solutions based on our CCD observations. Then, we compare our results with those from the other investigators. The orbital period changes are reinvestigated with new eclipse times together with the others collected from the literature. Finally, the formation and the evolutionary state of the system, as well as the probability of the additional companion orbiting around the contact binary, are all discussed.

2 CCD photometric observations

The first observations in the *V*-band with new times of two light minima were obtained with the 2.15 m "Jorge Sahade" (JS) telescope at Complejo Astronomico El Leoncito (CASLEO), San Juan, Argentina during 2011 December 9, 11, and 13. During the observations, a VersArray 1300B camera was attached to the 2.15 m telescope, producing 1095, 1300, and 1000 images on 2011 December 9, 11, and 13, respectively. The second

Table 1. Coordinates of RW Dor and the comparison and check stars.

Target	Names	$\alpha_{J2000.0}$	$\delta_{J2000.0}$	V	R	J	H	K
Variable star	RW Dor	$05^h18^m32\!\!.\!\!^s5$	$-68°13'32\!\!.\!\!''7$	11.16	8.66	9.282	8.781	8.709
Comparison star	GSC 09162-00441	$05^h18^m43\!\!.\!\!^s6$	$-68°07'33\!\!.\!\!''7$	12.25	11.89	11.916	11.859	11.863
Check star	J05175264−6813241	$05^h17^m52\!\!.\!\!^s6$	$-68°13'24\!\!.\!\!''1$	12.33	11.27	10.782	10.285	10.169
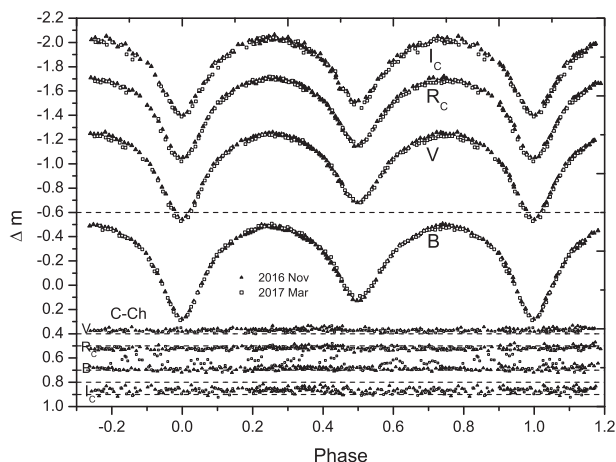
Fig. 1. Two sets for the second observation with complete light curves in the B, V, R_C, and I_C bands were obtained with the 0.6 m telescope at CTIO in 2016 November (black triangles) and 2017 March (open squares). The differential magnitude between the comparison and check stars in the BVR_CI_C bands (C − Ch) are plotted at the bottom of the figure and were used to calibrate all the data sets in each band.

observations in the $B, V, R_C I_C$ bands were obtained between 2015 March and 2017 March by using the back-illuminated Apogee F42 2048 × 2048 CCD photometric system attached to the 0.60 m Cassegrain reflecting telescope of the PROMPT-8[1] robotic telescope, which is located at the Cerro Tololo Inter-American Observatory (CTIO) in Chile. It also provided nightly calibration images, including bias, dark, and flat-field images (Layden & Broderick 2010). The CCD reduction and aperture photometry were done with standard procedure packages of IRAF.[2] The comparison star (C) was GSC 09162-00441 [$V = 12.25$, $J - H = 0.057$ (SIMBAD)] and the check star (Ch) was 2MASS J05175264−6813241 [$V = 12.33$, $J - H = 0.497$ (SIMBAD)]. The coordinates of those targets are listed in table 1, and the complete multi-color light curves for the second observation in 2016 November and 2017 March are displayed by black triangles and open squares, respectively, in figure 1. The data from figure 1 are listed in table 2 for 2016 and table 3 for 2017. A comparison of the two sets of light curves are also plotted together in the figure;

they nearly overlap, indicating that the light curves have no changes and are quite symmetric. This means that the light curves for our observations at this time are stable, which is the opposite of some results from previous investigators who found that the light curves showed asymmetry and varied with time. The depths of the primary and secondary minima of the two sets of light curves from figure 1 are given in table 4, and no significant changes were found there. This helps to confirm that the light curves have no variations or asymmetry from the O'Connell effect (O'Connell 1951) caused by spot or magnetic activities which normally occur, being similar to the Sun or late-type stars, e.g., spectral type F, G, and K.

3 Orbital period investigations

The orbital period changes were analyzed using the $O - C$ value. All the available eclipse times from the literature were collected and investigated together with new CCD photometric times from the present observations as listed in table 5. The $O - C$ values of those eclipse times were computed using the linear ephemeris given by Kreiner (2004):

$$\text{Min.I(HJD)} = 2451869.076 + 0.2854633E, \quad (1)$$

where Min.I denotes the primary light minimum at phase = 0.0 and E the cycle count after an estimated epoch. To analyze the $O - C$ changes, we first used a quadratic ephemeris to fit the $O - C$ curve with weight 1 for photographic data (pg) and weight 10 for photoelectric (pe) or CCD data. The result is plotted as the solid line in the upper panel of figure 2. A least-squares solution leads to the following quadratic ephemeris:

$$\begin{aligned} \text{Min.I(HJD)} = {} & 2451869.07751(\pm 0.00004) \\ & + 0.285462985(\pm 0.000000002)E \\ & - [55.5(\pm 0.2) \times 10^{-13}]E^2. \end{aligned} \quad (2)$$

From the quadratic term in equation (2), the orbital period is decreasing and the change rate can be determined as $dP/dt = -14.19(\pm 0.05) \times 10^{-9} \,\text{d yr}^{-1}$. The residuals from equation (2) are plotted in the lower panel of figure 2. As shown in figure 2, we found that a parabolic curve may not fit well; a cyclic variation seems to exist which can be seen clearly from the residuals in the lower panel that show a

---

[1] PROMPT-8 is the Thai Southern Hemisphere Telescope (TST), operated in collaboration between the National Astronomical Research Institute of Thailand (NARIT) and the University of North Carolina (UNC) at Chapel Hill as part of the UNC-led PROMPT project ⟨http://skynet.unc.edu⟩.

[2] The Image Reduction and Analysis Facility (IRAF): ⟨http://iraf.noao.edu⟩.

Table 2. CCD observations of RW Dor in 2016 November.

HJD (2457700+)	ΔV	HJD	ΔR	HJD	ΔI	HJD	ΔV	HJD	ΔR	HJD	ΔI
20.5558	−1.228	20.5562	−1.641	20.5566	−2.017	20.8129	−1.061	20.8134	−1.522	20.8138	−1.894
20.5585	−1.233	20.5589	−1.664	20.5593	−1.991	20.8151	−1.090	20.8155	−1.531	20.8159	−1.906
20.5612	−1.238	20.5616	−1.681	20.5619	−2.039	20.8172	−1.099	20.8177	−1.539	20.8180	−1.918
20.5637	−1.250	20.5642	−1.676	20.5646	−2.037	20.8193	−1.116	20.8198	−1.557	20.8202	−1.928
20.5667	−1.255	20.5672	−1.692	20.5675	−2.039	20.8213	−1.117	20.8218	−1.567	20.8223	−1.921
20.5696	−1.260	20.5701	−1.686	20.5706	−2.023	20.8235	−1.147	20.8240	−1.580	20.8244	−1.949
20.5727	−1.238	20.5731	−1.675	20.5735	−2.029	20.8267	−1.158	20.8272	−1.604	20.8276	−1.965
20.5756	−1.234	20.5760	−1.688	20.5764	−2.012	20.8289	−1.183	20.8294	−1.633	20.8298	−1.987
20.5784	−1.232	20.5789	−1.659	20.5793	−2.015	20.8307	−1.194	20.8312	−1.648	20.8316	−1.990
20.5814	−1.225	20.5818	−1.656	20.5822	−2.042	21.5639	−1.271	21.5643	−1.709	21.5648	−2.039
20.5842	−1.210	20.5845	−1.656	20.5849	−2.003	21.5668	−1.265	21.5673	−1.704	21.5677	−2.054
20.5868	−1.220	20.5873	−1.656	20.5877	−1.966	21.5700	−1.265	21.5704	−1.687	21.5709	−2.015
20.5897	−1.190	20.5902	−1.630	20.5907	−1.978	21.5729	−1.264	21.5735	−1.688	21.5739	−2.024
20.5926	−1.175	20.5931	−1.613	20.5936	−1.973	21.5760	−1.282	21.5763	−1.677	21.5767	−2.067
20.5957	−1.170	20.5961	−1.608	20.5964	−1.957	21.5789	−1.256	21.5793	−1.687	21.5798	−2.042
20.5984	−1.137	20.5988	−1.601	20.5991	−1.921	21.5820	−1.249	21.5824	−1.663	21.5828	−2.012
20.6012	−1.123	20.6017	−1.573	20.6021	−1.901	21.5851	−1.220	21.5856	−1.661	21.5860	−1.979
20.6080	−1.077	20.6085	−1.507	20.6089	−1.861	21.5882	−1.220	21.5887	−1.629	21.5892	−1.994
20.6110	−1.049	20.6115	−1.491	20.6119	−1.821	21.5914	−1.194	21.5919	−1.628	21.5923	−2.003
20.6140	−0.984	20.6144	−1.463	20.6148	−1.815	21.5945	−1.184	21.5950	−1.605	21.5954	−1.954
20.6170	−0.975	20.6175	−1.401	20.6179	−1.783	21.5975	−1.172	21.5980	−1.609	21.5984	−1.921
20.6201	−0.927	20.6205	−1.373	20.6208	−1.709	21.6006	−1.138	21.6011	−1.579	21.6015	−1.913
20.6229	−0.855	20.6233	−1.311	20.6237	−1.618	21.6036	−1.114	21.6040	−1.560	21.6043	−1.876
20.6259	−0.845	20.6264	−1.256	20.6267	−1.613	21.6095	−1.050	21.6100	−1.483	21.6103	−1.846
20.6291	−0.757	20.6295	−1.223	20.6298	−1.597	21.6124	−1.016	21.6129	−1.453	21.6133	−1.818
20.6321	−0.735	20.6326	−1.184	20.6329	−1.526	21.6156	−0.952	21.6159	−1.394	21.6164	−1.746
20.6352	−0.694	20.6357	−1.126	20.6361	−1.512	21.6188	−0.897	21.6192	−1.351	21.6197	−1.680
20.6384	−0.682	20.6388	−1.130	20.6393	−1.520	21.6219	−0.828	21.6224	−1.285	21.6228	−1.615
20.6414	−0.686	20.6419	−1.160	20.6423	−1.480	21.6250	−0.772	21.6255	−1.220	21.6259	−1.584
20.6446	−0.727	20.6451	−1.177	20.6454	−1.548	21.6285	−0.696	21.6290	−1.145	21.6295	−1.522
20.6477	−0.752	20.6483	−1.217	20.6486	−1.597	21.6317	−0.645	21.6322	−1.085	21.6325	−1.470
20.6509	−0.809	20.6513	−1.268	20.6517	−1.624	21.6349	−0.583	21.6354	−1.055	21.6358	−1.427
20.6540	−0.852	20.6545	−1.330	20.6549	−1.698	21.6384	−0.561	21.6389	−1.052	21.6394	−1.417
20.6573	−0.902	20.6576	−1.379	20.6581	−1.733	21.6417	−0.590	21.6421	−1.059	21.6425	−1.441
20.6603	−0.935	20.6608	−1.419	20.6612	−1.751	21.6450	−0.636	21.6455	−1.116	21.6458	−1.524
20.6636	−1.010	20.6639	−1.450	20.6644	−1.838	21.6482	−0.706	21.6487	−1.179	21.6491	−1.573
20.6668	−1.040	20.6673	−1.489	20.6677	−1.850	21.6515	−0.780	21.6519	−1.235	21.6524	−1.613
20.6701	−1.068	20.6706	−1.530	20.6709	−1.892	21.6548	−0.857	21.6553	−1.306	21.6557	−1.680
20.6732	−1.096	20.6737	−1.552	20.6741	−1.883	21.6582	−0.917	21.6586	−1.373	21.6591	−1.710
20.6765	−1.123	20.6769	−1.589	20.6773	−1.915	21.6616	−0.970	21.6621	−1.430	21.6625	−1.819
20.6797	−1.134	20.6802	−1.574	20.6806	−1.968	21.6637	−1.017	21.6642	−1.459	21.6646	−1.849
20.6830	−1.168	20.6835	−1.616	20.6839	−1.978	21.6670	−1.058	21.6675	−1.501	21.6678	−1.862
20.6863	−1.188	20.6868	−1.625	20.6870	−1.973	21.6703	−1.080	21.6708	−1.547	21.6713	−1.892
20.6894	−1.212	20.6899	−1.632	20.6904	−1.978	21.6738	−1.116	21.6742	−1.572	21.6747	−1.911
20.6928	−1.205	20.6932	−1.646	20.6936	−1.982	21.6773	−1.135	21.6778	−1.583	21.6782	−1.938
20.6961	−1.227	20.6966	−1.685	20.6970	−2.002	21.6793	−1.159	21.6797	−1.610	21.6802	−1.936
20.6994	−1.242	20.6998	−1.690	20.7002	−2.026	21.6827	−1.177	21.6832	−1.631	21.6837	−1.998
20.7026	−1.260	20.7031	−1.669	20.7036	−2.048	21.6863	−1.213	21.6868	−1.649	21.6872	−2.000
20.7060	−1.259	20.7065	−1.676	20.7069	−2.031	21.6898	−1.221	21.6903	−1.664	21.6906	−1.957
20.7080	−1.251	20.7085	−1.700	20.7089	−2.006	21.6917	−1.214	21.6922	−1.663	21.6926	−2.030
20.7538	−1.013	20.7542	−1.485	20.7546	−1.814	21.6938	−1.228	21.6944	−1.675	21.6948	−2.030
20.7563	−0.987	20.7568	−1.419	20.7573	−1.777	21.6959	−1.247	21.6964	−1.668	21.6969	−2.002
20.7591	−0.960	20.7596	−1.378	20.7601	−1.749	21.6979	−1.242	21.6985	−1.683	21.6989	−2.047
20.7617	−0.906	20.7621	−1.355	20.7625	−1.703	21.7003	−1.254	21.7008	−1.691	21.7013	−2.032

Table 2. (Continued)

HJD (2457700+)	ΔV	HJD	ΔR	HJD	ΔI	HJD	ΔV	HJD	ΔR	HJD	ΔI
20.7651	-0.828	20.7656	-1.299	20.7660	-1.615	21.7028	-1.260	21.7032	-1.685	21.7037	-2.031
20.7895	-0.656	20.7900	-1.141	20.7904	-1.495	21.7050	-1.261	21.7055	-1.705	21.7059	-2.024
20.7915	-0.676	20.7920	-1.153	20.7923	-1.530	21.7075	-1.263	21.7081	-1.713	21.7084	-2.065
20.7937	-0.724	20.7942	-1.199	20.7946	-1.558	21.7099	-1.265	21.7104	-1.694	21.7108	-2.035
20.7970	-0.808	20.7975	-1.254	20.7980	-1.643	21.7122	-1.265	21.7127	-1.709	21.7131	-2.078
20.8002	-0.869	20.8007	-1.330	20.8010	-1.710	21.7145	-1.268	21.7150	-1.709	21.7155	-2.047

large systematic scatter. Therefore, to get a better fit for the trend of $O - C$, a sinusoidal term is added to a quadratic ephemeris. By using a least-squares method, the ephemeris is redetermined as

$$
\begin{aligned}
\text{Min.I(HJD)} = {} & 2451869.07786(\pm 0.00004) \\
& + 0.285463214(\pm 0.000000007)E \\
& - [37.6(\pm 0.5) \times 10^{-13}]E^2 \\
& + 0.0054(\pm 0.0001) \\
& \times \sin[0°\!.00564E + 185°\!.824(\pm 0°\!.684)]. \quad (3)
\end{aligned}
$$

As shown in figure 3, equation (3) can give a good description of the general trend of the $O - C$ curve. After the downward parabolic change is subtracted, the cyclic oscillation is displayed in the middle panel. From this ephemeris, the sinusoidal term suggests that the semi-amplitude of cyclic variation is about 0.0054 d, while it has a long period of 49.92 yr. The quadratic term also reveals a continuous decrease at a rate of $dP/dt = -9.61(\pm 0.13) \times 10^{-9} \, \text{d yr}^{-1}$ that is smaller than that derived from equation (2). The residuals from equation (3) are also plotted in the bottom panel of figure 3. Its scatters are smaller than those in figure 2, which can be justified by the sum of weighted squares deviation of 0.000851 for equation (2) without a cyclical term and 0.000462 for equation (3) with a cyclical term, respectively.

However, it cannot be concluded that the result from figure 3 is better and more reliable than figure 2 because of the small number of $O - C$ data that do not cover (the gap between 1943 and 1980 or about 36.64 yr) the whole cycles. Furthermore, the period of the third body from figure 3 is 49.92 yr, while the total time span of available eclipse times is only 127.48 yr. Besides, the first nine minima (pre-1944) are photographic (pg), listed in table 3 to only three decimal places, and thus they have ten times smaller weights when compared to the photoelectric (pe) and CCD data. Consequently, the effective time span of higher-quality minima (pe and CCD data) is only 37 yr, less than the third body orbit period. Moreover, the point density (9 minima over a time interval of 53.81 yr) for the first group is much lower than

that of the second group (69 minima over a time interval of 37 yr). For these reasons, the evidence for a sinusoidal term in figure 3 is very weak. The result from equation (2) may be a possible explanation of the period change in the RW Dor system. However, to check the period changes proposed here, more eclipse times are still required in the future to confirm the period variations.

4 Photometric solutions

As shown in figure 1, the two sets of light curves obtained in 2016 November and 2017 March nearly overlap. This suggests that the light curves are stable within the error at that time interval, and no light curve variations from the O'Connell effect or spot activity cycles are found. However, the light curves of some close binaries are asymmetric, which could be explained by spot activity on one components or both (e.g., Qian et al. 2017a). For RW Dor, the light curves are quite symmetric indicating that they are very useful in determining the photometric solutions with high accuracy so that the more complicated solution of a spot model is not needed. We model the two sets of light curves separately: set-1 refers to the one observed on 2016 November 28–29 and set-2 refers to the other obtained on 2017 March 14–15. The two data sets in B, V, R_C, and I_C bands were analyzed separately by using the Wilson and Devinney (W–D) code (Wilson & Devinney 1971; Wilson 1990, 1994, 2012; van Hamme & Wilson 2007).

Hilditch, Hill, and Bell (1992) classified the spectral type of the binary as K1 V following Marton, Grieco, and Sistero (1989). The Tycho-2 mean color index $B - V = 0.66$ (Høg et al. 2000) corresponds to a spectral type of G4/5 V, while the color index in the SIMBAD database reveals a $B - V = 0.69$. For our solutions, the effective temperature of the primary star (T_1) was assumed to be 5560 K according to its spectral type (Cox 2000). We assume that the convective envelopes are already developed. Thus, the bolometric albedos for stars 1 and 2 were taken as $A_1 = A_2 = 0.5$, and the values of the gravity-darkening coefficients $g_1 = g_2 = 0.32$ were used. The monochromatic and bolometric limb-darkening coefficients were taken with a logarithmic law from van Hamme's table (van Hamme

Table 3. CCD observations of RW Dor in 2017 March.

HJD +2457800	ΔV	HJD	ΔR	HJD	ΔI	HJD	ΔV	HJD	ΔR	HJD	ΔI
26.5331	−0.871	26.5335	−1.338	26.5339	−1.683	26.6569	−1.095	26.6433	−1.626	26.6699	−1.719
26.5353	−0.837	26.5356	−1.290	26.5359	−1.663	26.6645	−1.007	26.6695	−1.410	26.6717	−1.703
26.5374	−0.806	26.5378	−1.261	26.5381	−1.633	26.6691	−0.919	26.6713	−1.310	27.5323	−1.642
26.5396	−0.789	26.5401	−1.227	26.5404	−1.575	26.6731	−0.826	27.5319	−1.251	27.5350	−1.593
26.5420	−0.766	26.5424	−1.223	26.5428	−1.553	27.5342	−0.725	27.5346	−1.179	27.5373	−1.540
26.5479	−0.737	26.5484	−1.190	26.5487	−1.525	27.5365	−0.703	27.5370	−1.142	27.5397	−1.506
26.5503	−0.761	26.5507	−1.221	26.5511	−1.572	27.5388	−0.638	27.5393	−1.124	27.5420	−1.497
26.5526	−0.781	26.5530	−1.240	26.5534	−1.586	27.5412	−0.625	27.5416	−1.098	27.5450	−1.464
26.5548	−0.811	26.5552	−1.282	26.5556	−1.617	27.5443	−0.593	27.5447	−1.070	27.5511	−1.499
26.5571	−0.843	26.5575	−1.320	26.5579	−1.671	27.5503	−0.624	27.5507	−1.136	27.5537	−1.551
26.5593	−0.859	26.5596	−1.347	26.5600	−1.709	27.5529	−0.675	27.5533	−1.164	27.5564	−1.589
26.5639	−0.951	26.5642	−1.402	26.5646	−1.778	27.5556	−0.724	27.5561	−1.192	27.5591	−1.681
26.5659	−0.983	26.5662	−1.428	26.5666	−1.791	27.5583	−0.794	27.5588	−1.259	27.5619	−1.691
26.5680	−1.020	26.5684	−1.456	26.5688	−1.823	27.5611	−0.855	27.5615	−1.322	27.5646	−1.753
26.5700	−1.023	26.5705	−1.490	26.5708	−1.840	27.5637	−0.929	27.5642	−1.381	27.5672	−1.795
26.5728	−1.068	26.5732	−1.518	26.5736	−1.879	27.5665	−0.969	27.5668	−1.436	27.5699	−1.811
26.5748	−1.091	26.5753	−1.553	26.5756	−1.903	27.5691	−1.014	27.5695	−1.481	27.5722	−1.907
26.5776	−1.134	26.5781	−1.558	26.5784	−1.906	27.5714	−1.046	27.5719	−1.507	27.5746	−1.867
26.5804	−1.148	26.5808	−1.600	26.5812	−1.965	27.5738	−1.071	27.5742	−1.557	27.5769	−1.924
26.5824	−1.150	26.5828	−1.609	26.5831	−1.950	27.5761	−1.105	27.5765	−1.556	27.5792	−1.946
26.5845	−1.160	26.5849	−1.617	26.5853	−1.997	27.5784	−1.132	27.5789	−1.576	27.5815	−1.961
26.5868	−1.182	26.5872	−1.627	26.5876	−2.002	27.5808	−1.152	27.5811	−1.591	27.5838	−1.965
26.5916	−1.219	26.5919	−1.659	26.5923	−2.014	27.5830	−1.159	27.5834	−1.617	27.5863	−2.007
26.5935	−1.211	26.5940	−1.661	26.5942	−1.983	27.5853	−1.194	27.5858	−1.636	27.5975	−2.034
26.5954	−1.224	26.5958	−1.687	26.5960	−2.063	27.5967	−1.228	27.5971	−1.693	27.6002	−2.076
26.5976	−1.250	26.5980	−1.694	26.5984	−2.041	27.5994	−1.250	27.5998	−1.720	27.6030	−2.061
26.5998	−1.227	26.6002	−1.686	26.6006	−2.043	27.6021	−1.264	27.6025	−1.743	27.6058	−2.084
26.6022	−1.250	26.6025	−1.710	26.6028	−2.049	27.6049	−1.270	27.6054	−1.725	27.6083	−2.110
26.6044	−1.258	26.6049	−1.708	26.6052	−2.076	27.6077	−1.292	27.6081	−1.736	27.6111	−2.120
26.6067	−1.266	26.6071	−1.708	26.6074	−2.093	27.6102	−1.302	27.6107	−1.733	27.6133	−2.095
26.6089	−1.266	26.6092	−1.709	26.6096	−2.079	27.6125	−1.304	27.6130	−1.752	27.6169	−2.108
26.6110	−1.282	26.6114	−1.725	26.6117	−2.094	27.6162	−1.302	27.6165	−1.768	27.6191	−2.115
26.6132	−1.283	26.6137	−1.705	26.6140	−2.086	27.6183	−1.302	27.6187	−1.765	27.6214	−2.110
26.6155	−1.279	26.6159	−1.714	26.6162	−2.057	27.6206	−1.290	27.6211	−1.742	27.6276	−2.085
26.6177	−1.282	26.6182	−1.721	26.6186	−2.069	27.6268	−1.307	27.6272	−1.752	27.6299	−2.090
26.6201	−1.284	26.6204	−1.718	26.6208	−2.085	27.6291	−1.280	27.6295	−1.731	27.6322	−2.069
26.6223	−1.283	26.6228	−1.711	26.6231	−2.074	27.6314	−1.277	27.6318	−1.722	27.6349	−2.052
26.6268	−1.272	26.6249	−1.730	26.6253	−2.066	27.6341	−1.256	27.6346	−1.735	27.6371	−2.082
26.6291	−1.253	26.6273	−1.719	26.6276	−2.046	27.6363	−1.264	27.6367	−1.703	27.6393	−2.085
26.6313	−1.246	26.6295	−1.718	26.6321	−2.066	27.6408	−1.232	27.6389	−1.698	27.6415	−2.032
26.6336	−1.261	26.6317	−1.704	26.6391	−2.044	27.6430	−1.261	27.6413	−1.682	27.6438	−1.990
26.6382	−1.229	26.6340	−1.686	26.6437	−1.967	27.6666	−1.052	27.6435	−1.656	27.6484	−2.022
26.6406	−1.192	26.6387	−1.667	26.6485	−1.925	27.6689	−0.987	27.6480	−1.720	27.6521	−1.977
26.6428	−1.188	26.6410	−1.677	26.6507	−1.957						

1993). All the fixed parameters are listed in table 4. The adjustable parameters are the inclination (i), the mass ratio (q), the temperature of star 2 (T_2), the monochromatic luminosity of star 1 (L_{1B}, L_{1V}, L_{1R_C}, and L_{1I_C}), and the dimensionless potential of star 1 ($\Omega_1 = \Omega_2$) in mode 3 for contact configuration.

For a precise mass ratio determination, Hilditch, Hill, and Bell (1992) published results of radial-velocity measurements and gave a mass ratio of $q_{sp} = 0.68 \pm 0.03$. Later, Duerbeck and Rucinski (2007) obtained $q_{sp} = 0.63 \pm 0.03$. However, we used a q-search method first with our photometric data to determine the photometric mass ratio

Table 4. Depths of eclipse (differential magnitude) in each band.

Filters	2016 Nov (pri, sec)	2017 Mar (pri, sec)
ΔB (± 0.004)	0.280, 0.127	0.288, 0.089
ΔV (± 0.002)	$-0.541, -0.682$	$-0.536, -0.681$
$\Delta R_{\rm C}$ (± 0.002)	$-1.052, -1.158$	$-1.033, -1.151$
$\Delta I_{\rm C}$ (± 0.003)	$-1.402, -1.491$	$-1.389, -1.487$

($q_{\rm ph}$) and then set the mass ratio as an adjustable parameter to get a better fit for the data in set-1 and set-2. We obtained the initial mass ratio at $q = 1.6$ ($q > 1.0$ for W-subtype) and then the differential correction was performed until the final solutions were derived at the lowest sum of the weighted square deviations $\Sigma[W(O-C)]^2$, hereafter Σ. The result is about q (W-subtype) $= 1.62 \pm 0.02$ or $q = 0.615$ in general meaning—which is close to the spectroscopic mass ratio of 0.63 derived by Duerbeck and Rucinski (2007)—for both data sets when the more massive component of the W-subtype system is the cooler. However, it is obvious that both sets of light curves show partial eclipses ($i < 85°$) so that their photometric mass ratios obtained by q-search may not be accurate, as discussed by Terrell and Wilson (2005). Therefore, we used the spectroscopic mass ratio of 0.63 or q (W-subtype) $= 1.587$ for our fixed mass ratio in the modeling process. The light-curve modeling results with optimum parameters are listed in table 6. The corresponding theoretical light curves (solid lines) were compared with the observed light curves as shown in figure 4 for the data in set-1 (left panel) and set-2 (right panel). Additionally, figure 3 shows a cyclic variation that may be caused by the light travel-time effect via the presence of a third body. Therefore, we added the third light (l_3) as an adjustable parameter in order to check the luminosity contribution of such a third companion, but the results show negative values for both data sets. This may suggest that if the third body really exists, it will be a very cool stellar companion. On the other hand, it may have no companion orbiting the eclipsing pair. The presence of the third body is discussed again in the next section. The geometrical structures of RW Dor based on the modeling are displayed in figure 5.

5 Discussions and conclusions

The two sets of complete multi-color light curves in the BVR_CI_C bands were obtained by using the PROMPT-8 robotic telescope at CTIO in Chile between 2015 March and 2017 March. The other data in 2011 were obtained by using the 2.15 m telescope at CASLEO, San Juan, in Argentina. We compared our results with the light curves published by Deb and Singh (2011): no O'Connell

effect or light curve variations were found. The photometric solutions indicate that RW Dor is a W-subtype, shallow contact binary with a degree of contact more than 10% and a high mass ratio q (W-subtype) ~ 1.587 or $q = 0.63$ in general meaning, which indicates that the hotter component is the less massive one. The absolute dimensions of RW Dor derived by using our photometric elements together with spectroscopic ones by Duerbeck and Rucinski (2007) are: $M_1 = 0.52\,M_\odot$, $M_2 = 0.82\,M_\odot$, $a = 2.03\,R_\odot$, $R_1 = 0.703\,R_\odot$, $R_2 = 0.881\,R_\odot$, $L_1 = 0.423\,L_\odot$, and $L_2 = 0.534\,L_\odot$. These parameters are close to those recently derived by Deb and Singh (2011).

The downward parabolic curve in the $O - C$ diagram shows an orbital period decrease at a rate of $dP/dt = -14.19 \times 10^{-9}\,{\rm d\,yr^{-1}}$ without a sinusoidal term and $dP/dt = -9.61 \times 10^{-9}\,{\rm d\,yr^{-1}}$ with a cyclical term. The type of variations, i.e., a long-term decrease combined with a cyclic change, is commonly found in W UMa-type stars, for example V417 Aql (Qian 2003), V1139 Cas (Li et al. 2015b), MR Com (Qian et al. 2013b), BX Peg (Li et al. 2015a), V524 Mon (He et al. 2012), and V1073 Cyg (Tian et al. 2018). Some W-type contact binaries whose properties are similar to RW Dor are listed in table 8: most of them are shallow contact binaries with decreasing period. The long-term decrease in period can be explained either by mass transfer from the more massive component to the less massive one or by angular momentum loss (AML) via magnetic braking, or by a combination of both processes. If the long-term decrease in period is due to conservative mass transfer, the mass transfer rate can be determined with the following equation (Kwee 1958):

$$\frac{\dot{P}}{P} = -3\dot{M}_2\left(\frac{1}{M_1} - \frac{1}{M_2}\right). \tag{4}$$

The mass transfer rate is $dM/dt = 23.55 \times 10^{-9}\,M_\odot\,{\rm yr^{-1}}$ without a cyclical term and $dM/dt = 15.95 \times 10^{-9}\,M_\odot\,{\rm yr^{-1}}$ with a cyclical term. The timescale of mass transfer can be computed as $M_2/\dot{M} \sim 3.48 \times 10^7\,{\rm yr}$ (or 35 Myr) for equation (2) and $M_2/\dot{M} \sim 5.14 \times 10^7\,{\rm yr}$ (or 51 Myr) for equation (3), while the timescale of the period decrease is $P/\dot{P} \sim 2.01 \times 10^7\,{\rm yr}$ (or 20 Myr) without a sinusoidal term and $P/\dot{P} \sim 2.97 \times 10^7\,{\rm yr}$ (or 30 Myr) with a sinusoidal term. The thermal timescale of the more massive component is $46.43 \times 10^6\,{\rm yr}$ (or 46 Myr). These timescales reveal that RW Dor is presently undergoing a slow mass transfer at the beginning stages of contact evolution with a high mass ratio, shallow contact configuration, and long-term decrease in the orbital period. In this way, the contact degree of the system will become higher and the system will evolve into a deeper contact binary. Another plausible

Table 5. Times of light minima for RW Dor.

HJD (2400000+)	Error (d)	Method	Min. (type)	Ref.	HJD (2400000+)	Error (d)	Method	Min. (type)	Ref.*
11298.835		pg	II	(1)	46681.7865	0.001	pe	II	(5)
14168.883		pg	II	(1)	46690.7785	0.0001	pe	I	(6)
15621.901		pg	II	(1)	46695.7745	0.0001	pe	II	(6)
16013.836		pg	II	(1)	48500.0470			I	(10)
16489.714		pg	II	(1)	50559.9437	0.0004	ccd	I	(7)
17075.903		pg	I	(1)	50560.0865	0.0003	ccd	II	(7)
23784.600		pg	I	(1)	51158.5603	0.0002	ccd	I	(7)
24172.537		pg	I	(1)	51158.7027	0.0002	ccd	II	(7)
30938.602		pg	I	(10)	51505.6820	0.0002	ccd	I	(7)
44313.581	0.001	pe	II	(2)	51505.8252	0.0002	ccd	II	(7)
44464.876	0.001	pe	II	(2)	51548.5020		ccd	I	(10)
44581.7728	0.0008	pe	I	(2)	51869.0760		ccd	I	(10)
44608.6063	0.0005	pe	I	(2)	54036.5947		ccd	I	(10)
44608.7488	0.0006	pe	II	(2)	54036.7411		ccd	II	(10)
44609.6063	0.0008	pe	II	(2)	54037.5995		ccd	II	(10)
44609.7493	0.0005	pe	I	(2)	54037.7384		ccd	I	(10)
44610.7487	0.0009	pe	II	(2)	54041.7335		ccd	I	(10)
44825.8462	0.0008	pe	I	(3)	54049.5878		ccd	II	(10)
44826.8442	0.0004	pe	II	(3)	54059.7177		ccd	I	(10)
44873.8038	0.0006	pe	I	(3)	54087.9783	0.0001	pe	I	(8)
44874.6594	0.0003	pe	I	(3)	54091.1189	0.0002	pe	I	(8)
44874.8010	0.0004	pe	II	(3)	54095.1150	0.0001	pe	I	(8)
44958.5851	0.0004	pe	I	(3)	54107.6761		ccd	I	(10)
44961.5843	0.0006	pe	II	(3)	55904.66718	0.00005	ccd	I	(9)
44961.7239	0.0006	pe	I	(3)	55906.80840	0.00005	ccd	II	(9)
44962.5815	0.0007	pe	I	(3)	56950.7446		ccd	II	(10)
44962.7267	0.0005	pe	II	(3)	57112.6009	0.0001	ccd	II	(9)
45021.6738	0.0003	pe	I	(3)	57118.5968	0.0001	ccd	II	(9)
45049.5058	0.0006	pe	II	(3)	57446.7363	0.0001	ccd	I	(9)
45049.6486	0.0008	pe	I	(3)	57447.5930	0.0001	ccd	I	(9)
45050.6484	0.0003	pe	II	(3)	57644.8485	0.0002	ccd	I	(9)
45076.4815	0.0004	pe	I	(3)	57645.8477	0.0001	ccd	II	(9)
45370.6556	0.0001	pe	II	(4)	57661.8334	0.0002	ccd	II	(9)
45370.6558	0.0003	pe	II	(4)	57686.6689	0.0003	ccd	II	(9)
45370.6564	0.0004	pe	II	(4)	57686.8119	0.0002	ccd	I	(9)
45376.6502	0.0001	pe	II	(4)	57720.6390	0.0002	ccd	II	(9)
45376.6507	0.0002	pe	II	(4)	57721.6383	0.0002	ccd	I	(9)
45376.6517	0.0002	pe	II	(4)	57826.5461	0.0002	ccd	II	(9)
46680.7878	0.001	pe	I	(5)	57827.5454	0.0002	ccd	I	(9)

*References: (1) Hertzsprung ([1928](#)), (2) Marton and Grieco ([1981](#)), (3) Grieco and Marton ([1983](#)), (4) Russo, Vittone, and Milano ([1984](#)), (5) Marton, Grieco, and Sistero ([1989](#)), (6) Kaluzny and Caillault ([1989](#)), (7) Ogloza and Zakrzewski ([2004](#)), (8) Marino et al. ([2007](#)), (9) the present authors, (10) ⟨http://var.astro.cz/ocgate⟩.

explanation for the long-term decrease in period is AML via magnetic stellar wind, which can be determined by the following equation given by Bradstreet and Guinan (1994):

$$\dot{P} \approx -1.1 \times 10^{-8} q^{-1}(1+q)^2 (M_1 + M_2)^{-5/3} k^2$$
$$\times (M_1 R_1^4 + M_2 R_2^4) P^{-7/3}, \qquad (5)$$

where k^2 is the gyration constant ranging from 0.07 to 0.15 for solar-type stars. By adopting a value of

$k^2 = 0.1$ (Bradstreet & Guinan 1994), the rate of orbital period decrease due to AML can be computed as $dP/dt = -33.2 \times 10^{-9}\,\mathrm{d\,yr^{-1}}$: in this case the timescale of period decrease is $P/\dot{P} \sim 8.598 \times 10^6$ yr (or 8.6 Myr) which is about two times shorter than the timescale from equation (2) and three times shorter than that from equation (3). This means that the conservative mass transfer may not satisfactorily explain the secular decrease in period, or the mass transfer may be dynamical (Qian & Zhu 2002).
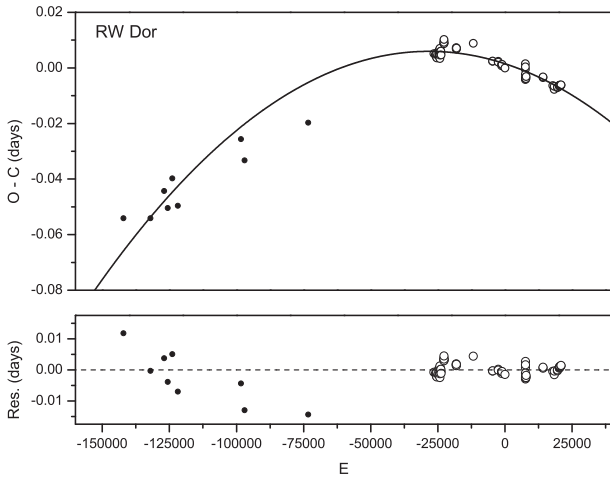
Fig. 2. ($O − C$) curve. The dots before $E = −50000$ refer to photographic data (pg) and the open circles after $E = −50000$ refer to photoelectric (pe) and CCD data. The solid line in the upper panel was computed by using the quadratic term in equation (2), and this downward parabolic curve suggests a long-term decrease in period. The residuals from equation (2) are plotted in the lower panel.
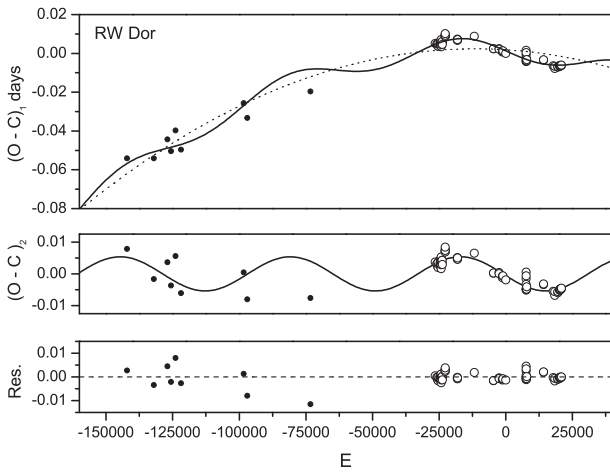

Fig. 3. ($O − C$)$_1$ diagram constructed by using the ephemeris in equation (1). The solid line in the upper panel refers to a combination of a long-term decrease in period and a small-amplitude cyclic variation, while the dashed line represents the long-term decrease of the orbital period. After subtracting the quadratic term, the result is displayed on the middle panel. The bottom panel shows the residuals for equation (3).

To explain this, Qian (2001a) proposed that the rate of AML is changed depending on the depth of overcontact. When the period decreases, the separation between the components becomes closer and the depth of contact increases, causing the common convective envelope (CCE) to become deeper and increase mixing in the CCE, which may result in AML at a lower rate (Vilhu 1981; Smith 1984). If the AML value is larger than the critical value of Rahunen (1981) and causes the orbital period to decrease, the evolution of RW Dor will be on the AML-controlled stage.

Table 6. Photometric solutions for the data in set-1 and set-2 when $T_1 = 5560$ K.

Parameters	set-1	set-2
T_1 (K)	5560 (assumed)	fixed
$g_1 = g_2$	0.32 (assumed)	fixed
$A_1 = A_2$	0.50 (assumed)	fixed
$q\,(M_2/M_1)$	1.587 (assumed)	fixed
T_2 (K)	5287 (±10)	5238 (±13)
$T_1 − T_2$ (K)	273 (±5)	322 (±6)
T_2/T_1	0.951 (±0.002)	0.942 (±0.002)
$i\,(°)$	77.2 (±0.1)	76.9 (±0.2)
Ω_{in}	3.091	3.091
Ω_{out}	2.732	2.732
$\Omega_1 = \Omega_2$	4.64 (±0.04)	4.62 (±0.03)
$L_1/(L_1 + L_2)\,(B)$	0.475 (±0.006)	0.491 (±0.006)
$L_1/(L_1 + L_2)\,(V)$	0.455 (±0.005)	0.467 (±0.005)
$L_1/(L_1 + L_2)\,(R_C)$	0.444 (±0.005)	0.455 (±0.005)
$L_1/(L_1 + L_2)\,(I_C)$	0.437 (±0.005)	0.446 (±0.004)
r_1 (pole)	0.3222 (±0.0013)	0.3242 (±0.0014)
r_1 (side)	0.3378 (±0.0014)	0.3402 (±0.0015)
r_1 (back)	0.3740 (±0.0015)	0.3777 (±0.0018)
r_2 (pole)	0.4057 (±0.0053)	0.4069 (±0.0048)
r_2 (side)	0.4309 (±0.0069)	0.4326 (±0.0063)
r_2 (back)	0.4635 (±0.0102)	0.4658 (±0.0093)
f	11.5% (±6.7%)	15.0% (±6.1%)
$\Sigma\, W_i (O − C)_i^2$	0.01641	0.01866

Based on period studies by Qian (2001a), the evolution of RW Dor may be a combination of thermal relaxation oscillation (TRO) and AML changes through the variable depth of overcontact, e.g., V417 Aql (Qian 2003). In addition, the study by Marton, Grieco, and Sistero (1989) has shown that there is a hot spot on the cooler component located near the neck of the system, suggesting a secondary-to-primary mass transfer which is in good agreement with the long-term decrease in period. This indicates that RW Dor is in the transition phase to W UMa and at the beginning of the contact phase, being similar to VW Boot (Qian & Zhu 2002). If the orbital-period decrease is caused by losing angular momentum through magnetic braking, this is in agreement with the conclusion derived by Qian et al. (2017b, 2018) that some EW-type contact binaries were formed from short-period EA-type systems via Case A mass transfer (Vilhu 1982; Bradstreet & Guinan 1994). Spectroscopic observations with LAMOST (Qian et al. 2017b, 2018) reveal that short-period EW binaries ($P < 0.4$ d) have low metallicities, suggesting that EW-type binaries are old stellar populations and may be older than their long-period cousins. This means that they have a longer pre-contact phase (Qian et al. 2017b). Moreover, the evolution study of low-mass contact binaries by Stepien and Gazeas (2012) indicates that systems with a low total mass ($M < 1.4\,M_\odot$)
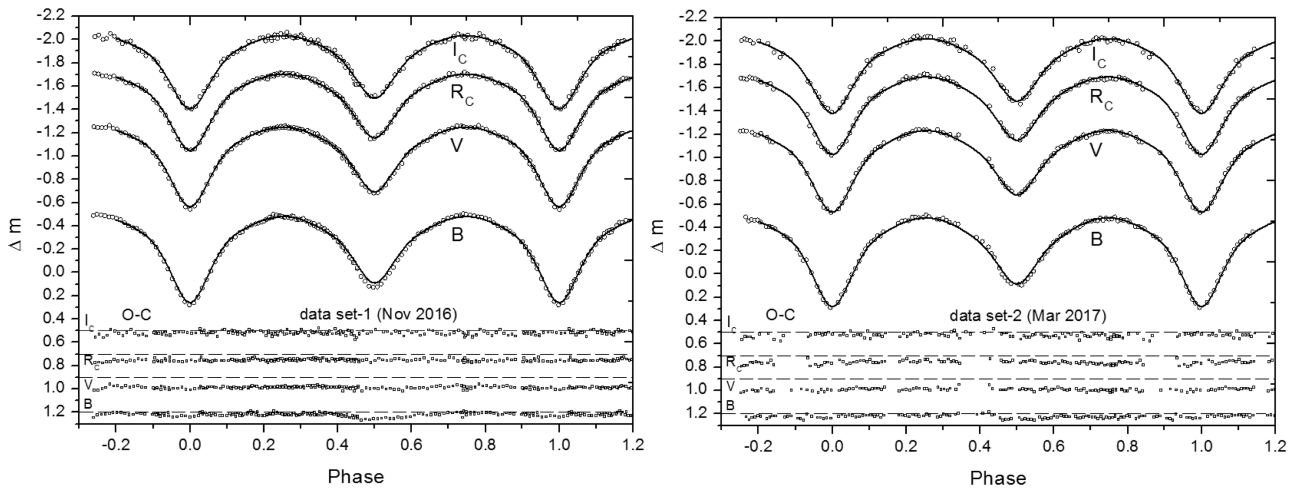
Fig. 4. Theoretical light curves (solid lines) computed by the W–D method compared with the observed light curves for the data in set-1 (left panel) and set-2 (right panel) without the third light and a spot. All theoretical light curves in $BVR_C I_C$ bands are fitted well to the observed light curves; this means that the physical parameters obtained from the light curve modeling are correct and reliable, except for the B-band light curves in set-1 which do not fit well at the secondary minimum.
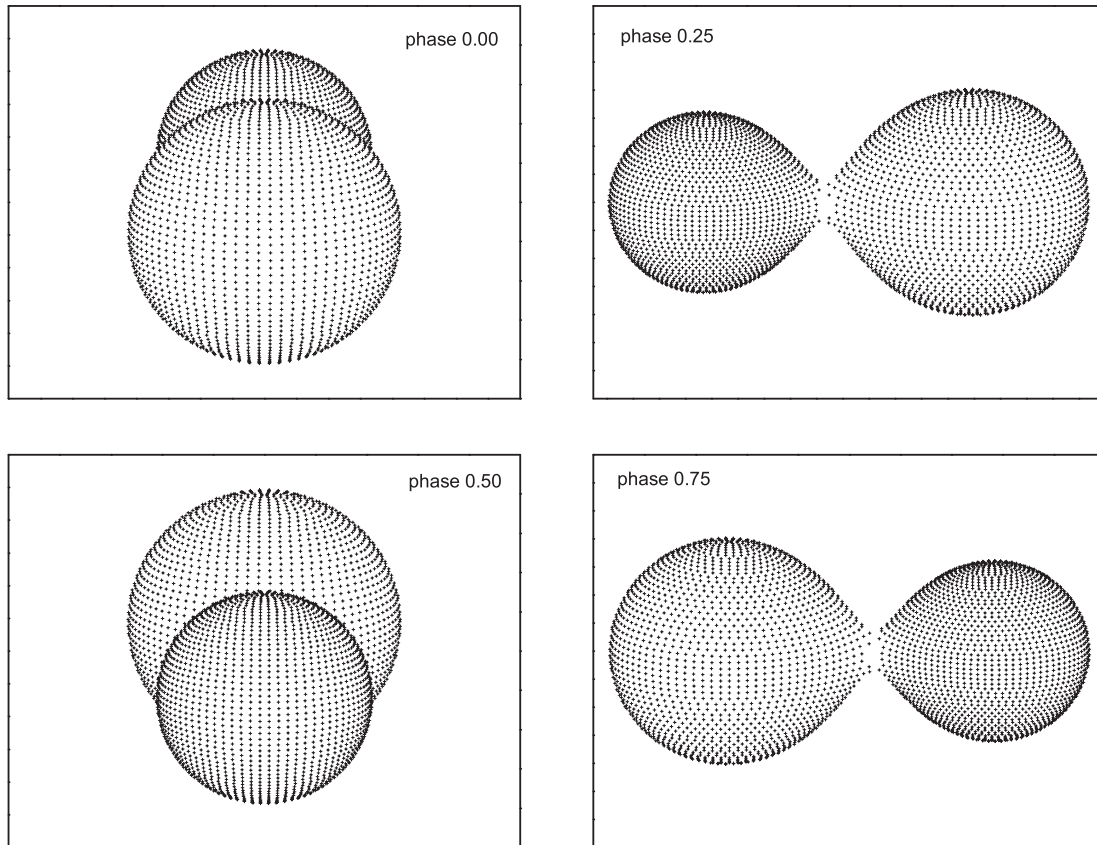
Fig. 5. Geometrical structures at phases of 0.00, 0.25, 0.50, and 0.75.

and a short orbital period ($P < 0.3$ d) have a long pre-contact phase that lasts for 8–9 Gyr, while the contact phase takes only about 0.8 Gyr with a low mass transfer rate. The situation of RW Dor is in good agreement with the conclusions proposed by Stepien and Gazeas (2012) and Qian

et al. (2017b, 2018) that a shallow-contact binary with a short period ($P \sim 0.285$ d), low total mass ($M \sim 1.34 M_\odot$), and long-term decrease in period is a newly formed contact binary, which is similar to V524 Mon (He et al. 2012), MR Com (Qian et al. 2013b), BI Vul (Qian et al. 2013a),

and CSTAR 038663 (Qian et al. 2014), at the beginning state of the contact phase or recently evolved into a contact configuration after it spent a long time in the pre-contact phase. In addition, the absolute parameters of RW Dor are quite close to V336 TrA (Kriwattanawong et al. 2018, their figure 4), suggesting that the more massive component (the secondary) of RW Dor will locate near the ZAMS (the zero-age main sequence), while the location of the less massive one should be close to the TAMS (the terminal-age main sequence). This means that the less massive one has evolved to reach the TAMS, whereas the more massive one has not evolved. This may be due to the mass transfer between the components.

In addition, a cyclic oscillation superimposed on a secular term is often found in W UMa-type binaries (see Qian 2001b, 2002). Furthermore, a study of the light travel-time effect in short-period eclipsing binaries by Li et al. (2018b) indicates that the frequency of third bodies found in contact binaries with a period shorter than 0.3 d reaches a value of 0.65 (65%) in their samples of 542 eclipsing binaries. Therefore, it is possible that there may exist a periodic variation superimposed on a secular decrease in period in the $O - C$ curve of RW Dor, even weak evidence as explained in section 3. If we assume that the periodic change in the $O - C$ curve exists, by analysis of equation (3) the sinusoidal term reveals a cyclic change with a semi-amplitude of 0.0054 d and a period of 49.92 yr. The periodic variations in W UMa binary stars are usually explained by two ideas: one is the Applegate mechanism (Applegate 1992) via magnetic activity cycles at one component or both, and the second idea is the light travel-time effect (Liao & Qian 2010; Han et al. 2016) via the presence of a third body.

The Applegate mechanism suggests that the cyclic change is caused by magnetic activity-driven variations in the quadrupole moment of solar-type components. Because RW Dor consists of G4/5 V spectral type stars, it should show strong magnetic activity. If this is the case, the quadrupole moment of the binary star can be determined from the equations given by Rovithis-Livaniou et al. (2000) and Lanza and Rodono (2002):

$$\Delta P = \sqrt{[1 - \cos(2\pi P / P_3)]} \times A_3, \qquad (6)$$

and

$$\frac{\Delta P}{P} = -9 \frac{\Delta Q}{M a^2}, \qquad (7)$$

where A_3 is the amplitude of the sinusoidal term in equation (3), P_3 is the magnetic activity period, R is the radius of the active star, and a is the separation. The result is $\Delta P / P \sim 1.317 \times 10^{-6}$, and the quadruple moment for the primary star is $\Delta Q_1 = 3.07 \times 10^{48} \, \mathrm{g \, cm^2}$ and that for the

Table 7. Parameters of the tertiary component for RW Dor.

Parameter	Value	Error	Units
P_3	49.9207	0.0003	yr
A_3	0.0054	**0.0001**	d
$a'_{12} \sin i'$	0.929	0.026	au
$f(m)$	0.00032	0.00003	$M_\odot$
e_3	0.0	assumed	—
$M_3 \, (i' = 90°)$	0.087	0.002	$M_\odot$
$a_3 \, (i' = 90°)$	14.33	0.58	au

secondary star is $\Delta Q_2 = 4.84 \times 10^{48} \, \mathrm{g \, cm^2}$. These values for both components are lower than the typical values for an active contact binary, which range from 10^{51} to $10^{52} \, \mathrm{g \, cm^2}$. Thus, the cyclic oscillation in figure 3 cannot be interpreted as the result of the Applegate mechanism. Furthermore, no spot activity cycles or light curve variations were found during the observations. The light curves may be stable for years (see figure 1) compared with the previous publications, which suggests that there is a very weak magnetic activity cycle at that time. Therefore, this period modulation may not be caused by a magnetic activity cycle that happens normally in single solar-type stars. There are many contact systems in which periodic variations cannot be explained by the Applegate mechanism, as discussed by Qian et al. (2013a), but the most probable reason causing the cyclic changes for those binaries is the light travel-time effect due to perturbations from a third body (Irwin 1952; Borkovits & Hegedues 1996; Liao & Qian 2010).

Therefore, a plausible idea for the cyclic period change is the light travel-time effect via the presence of a third body. By assuming that the tertiary component is moving in a circular orbit, the value of $a'_{12} \sin i'$ is computed as 0.929 au by using the relation $a'_{12} \sin i' = A_3 \times c$, where A_3 is the semi-amplitude of the $O - C$ oscillation, c is the speed of light, and i' is the orbital inclination of the third component. Thus, the mass function, the masses, and the orbital radii of the third component in different inclination values can be determined by solving the following equation:

$$f(m) = \frac{4\pi^2}{G P_3^2} \times (a'_{12} \sin i')^3 = \frac{(M_3 \sin i')^3}{(M_1 + M_2 + M_3)^2}; \qquad (8)$$

the corresponding values are displayed in table 7. The mass function of the third body can be derived as $f(m) = 0.00032(\pm 0.00003) \, M_\odot$. The mass of the third body is $M_3 \sin i' = 0.087(\pm 0.002) M_\odot$ and the orbital radius is $a_3 = 14.33$ au. If the minimum mass of the third body is $0.087 \, M_\odot$, the third body will be a very low-mass star, red dwarf, or M-type star with extremely small luminosity and hence is difficult to detect. Since no third light was reported in the photometric studies (Marino et al. 2007; Deb & Singh 2011) and no spectral lines of a third body were

Table 8. Parameters of marginal contact binaries (W-type systems).

Star	Sp.	Period (d)	$1/q$	f (%)	dP/dt ($\times 10^{-8}$ d yr^{-1})	Cyclic	l_3	M_1 ($M_\odot$)	M_2 ($M_\odot$)	M_3 ($M_\odot$)	Activities	Ref.*
KIC 9532219	G9	0.1981	0.833	—	−52.7	yes	76%	—	—	0.09	spot	(1)
CC Com	K4/5	0.2207	0.527	16.7	−20.0	yes	—	0.37	0.71	0.066	—	(2)
BI Vul	K3	0.2518	0.964	8.7	−9.5	yes	no	0.72	0.75	0.30	spot	(3)
V336 TrA	K1	0.2668	0.716	15.7	—	—	—	0.65	0.91	—	spot	(4)
CSTAR 038663	K3	0.2671	0.893	10.6	—	yes	<1%	0.72	0.81	0.63/2.02	spot/flares	(5)
BM UMa	K	0.2712	0.540	17.0	−7.49	yes	—	0.50	0.92	0.25	—	(6)
BX Peg	G5	0.2804	0.372	23.1	−9.84	yes	no	0.38	1.02	0.22	spot	(7)
GSC 2765-0348	G4	0.2835	0.313	34.0	—	—	—	—	—	—	2 spots	(8)
V524 Mon	G5	0.2836	0.476	7.7	−.015	yes	no	0.50	1.10	0.26	no	(9)
LO Com	K0	0.2864	0.404	3.2	−11.8	yes	no	0.32	0.79	—	no	(10)
GSC 3526-01995	K2	0.2922	0.351	18.2	—	yes	no	0.28	0.80	0.57	spot	(11)
IK Boo	G2	0.3031	0.873	2.2	−21.7	yes	—	0.86	0.99	0.21	spot	(12)
V2284 Cyg	G7	0.3069	0.345	39.2	−29.7	yes	no	0.30	0.86	0.036	no	(13)
TY Boo	G3	0.3171	0.466	12.0	−2.99	yes	—	0.53	1.14	0.49	—	(14)
V1007 Cas	K0	0.3320	0.297	8.1	−17.8	—	1.1%	0.34	1.14	—	spot	(15)
V781 Tau	G0	0.3449	0.453	21.6	−6.01	yes	no	0.71	1.57	0.16	spot	(16)
V396 Mon	F8	0.3963	0.392	18.9	−8.57	yes	no	0.36	0.92	0.31	—	(17)
PP Lac	G6	0.4012	0.435	23.9	—	yes	no	0.51	1.18	0.21	no	(18)
MR Com	F5	0.4127	0.256	10.0	−53.0	yes	<1%	0.36	1.40	0.18	no	(19)
RW Dor	G4/5	0.2854	0.630	>10	−1.42	unclear	no	0.52	0.82	unclear	no	(20)

*References: (1) Lee et al. (2016), (2) Yang et al. (2009a), (3) Qian et al. (2013a), (4) Kriwattanawong et al. (2018), (5) Qian et al. (2014), (6) Yang, Wei, and Nakajima (2009b), (7) Lee et al. (2004, 2009), (8) Samec et al. (2012), (9) He et al. (2012), (10) Zhang, Han, and Liu (2016), (11) Liao, Qian, and Liu (2012), (12) Kriwattanawong, Sanguansak, and Maungkorn (2017), (13) Wang et al. (2017), (14) Yang et al. (2007), (15) Li et al. (2018a), (16) Li et al. (2016), (17) Liu et al. (2011), (18) Qian, Zhu, and Boonruksar (2005), (19) Qian et al. (2013b), (20) the present study.

found (Rucinski et al. 2007), to check the third body we also searched for the third light during the photometric solution, but the results showed negative values which mean that the contribution of the third light is very small compared with the total light of the system. Since its minimum mass ($i' \sim 90°$) is small and it is located very far ($\sim$14.33 au) from the central binary system, it may not play an important role in the origin and evolution of the central binary by removing angular momentum from the inner system via the Kozai cycle (Kozai 1962). In this way, RW Dor will evolve normally into the contact phase without acceleration.

Based on section 3, there is very weak evidence for cyclic change in the $O − C$ analysis of figure 3 because of a few eclipse timings before 1948 with large scatter and a big gap of time between 1943 and 1980. However, almost contact binaries were found to be a triple or multiple system (Pribulla & Rucinski 2006; D'Angelo et al. 2006; Rucinski et al. 2007), and one can see from table 6 that most of them have no third light in their light curves but show periodic variations in long-term period changes. Recently, a possible substellar object orbiting the solar-like contact binary V2284 Cyg was first reported by Wang et al. (2017), and also in the K-type shallow contact binary CC Com with very low mass $M_3 = 0.066 M_\odot$ by Yang et al. (2009a), and KIC 9532219 with $M_3 = 0.089 M_\odot$ by Lee et al. (2016) or

TX Cnc with $M_3 = 0.097 M_\odot$ by Liu et al. (2007). More recently, the eclipsing binary Kepler-503 has been found to be a brown dwarf or low-mass star with $M_3 = 0.075 M_\odot$ orbiting around a subgiant star (Cañas et al. 2018). Therefore, the existence of a third body in the system cannot be ruled out completely. To prove whether or not the invisible additional companion exists, long-term photometric monitoring with new eclipse timings and spectroscopic observations are required.

Acknowledgments

References

Applegate, J. H. 1992, ApJ, 385, 621

Borkovits, T., & Hegedues, T. 1996, A&AS, 120, 63

Bradstreet, D. H., & Guinan, E. F. 1994, ASP Conf. Ser., 56, Interacting Binary Stars, ed. A. W. Shafter (San Francisco: ASP), 228

Cañas, C. I., et al. 2018, ApJ, 861, L4

Cannon, A. J. 1921, Harvard Coll. Obs. Bull., 754

Cox, A. N. 2000, Allen's Astrophysical Quantities, 4th ed. (New York: Springer)

D'Angelo, C., van Kerkwijk, M. H., & Rucinski, S. M. 2006, AJ, 132, 650

Deb, S., & Singh, H. P. 2011, MNRAS, 412, 1787

Duerbeck, H. W., & Rucinski, S. M. 2007, AJ, 133, 169

Grieco, A., & Marton, S. F. 1983, IBVS, 2436

Han, Z.-T., Qian, S.-B., Voloshina, I., Metlov, V. G., Zhu, L.-Y., & Li, L.-J. 2016, Res. Astron. Astrophys., 16, 156

He, J., & Qian, S. 2009, Ap&SS, 321, 209

He, J.-J., Wang, J.-J., & Qian, S.-B. 2012, PASJ, 64, 85

Hertzsprung, E. 1925, Bull. Astron. Inst. Netherlands, 2, 218

Hertzsprung, E. 1928, Bull. Astron. Inst. Netherlands, 4, 153

Hilditch, R. W., Hill, G., & Bell, S. A. 1992, MNRAS, 255, 285

Høg, E., et al. 2000, A&A, 355, L27

Irwin, J. B. 1952, ApJ, 116, 211

Kaluzny, J., & Caillault, J.-P. 1989, Acta Astron., 39, 27

Kozai, Y. 1962, AJ, 67, 579

Kreiner, J. M. 2004, Acta Astron., 54, 207

Kriwattanawong, W., Sanguansak, N., & Maungkorn, S. 2017, PASJ, 69, 62

Kriwattanawong, W., Sarotsakulchai, T., Maungkorn, S., Reichart, D. E., Haislip, J. B., Kouprianov, V. V., LaCluyze, A. P., & Moore, J. P. 2018, New Astron., 61, 1

Kwee, K. K. 1958, Bull. Astron. Inst. Netherlands, 14, 131

Lanza, A. F., & Rodono, M. 2002, AN, 323, 424

Layden, A. C., & Broderick, A. J. 2010, PASP, 122, 1000

Leavitt, H. S. 1908, Annal. Harvard Coll. Obs., 60, 109

Lee, J. W., Hong, K., Koo, J.-R., & Park, J.-H. 2016, ApJ, 820, 1

Lee, J. W., Kim, C.-H., Han, W.-Y., & Kim, H.-I. 2004, MNRAS, 352, 1041

Lee, J. W., Kim, S.-L., Lee, C.-U., & Youn, J.-H. 2009, PASP, 121, 1366

Li, K., Gao, D.-Y., Hu, S.-M., Guo, D.-F., Jiang, Y.-G., & Chen, X. 2016, Ap&SS, 361, 63

Li, K., Hu, S., Guo, D., Jiang, Y., Gao, D., & Chen, X. 2015a, New Astron., 41, 17

Li, K., Hu, S.-M., Guo, D.-F., Jiang, Y.-G., Gao, D.-Y., & Chen, X. 2015b, New Astron., 34, 217

Li, K., Xia, Q.-Q., Hu, S.-M., Guo, D.-F., & Chen, X. 2018a, PASP, 130, 074201

Li, M. C. A., et al. 2018b, MNRAS, 480, 4557

Liao, W.-P., & Qian, S.-B. 2010, MNRAS, 405, 1930

Liao, W.-P., Qian, S.-B., & Liu, N.-P. 2012, AJ, 144, 178

Liu, L., Qian, S.-B., Boonrucksar, S., Zhu, L.-Y., He, J.-J., & Yuan, J.-Z. 2007, PASJ, 59, 607

Liu, L., Qian, S.-B., Liao, W.-P., He, J.-J., Zhu, L.-Y., Li, L.-J., & Zhao, E.-G. 2011, AJ, 141, 44

Lucy, L. B., & Wilson, R. E. 1979, ApJ, 231, 502

McLaughlin, D. B. 1927, AJ, 38, 45

Marino, B. F., Walker, W. S. G., Bembrick, C., & Budding, E. 2007, PASA, 24, 199

Marton, F., & Grieco, A. 1981, IBVS, 1960

Marton, S. F., Grieco, A., & Sistero, R. F. 1989, MNRAS, 240, 931

O'Connell, D. J. K. 1951, Riverview Coll. Obs. Publ., 2, 85

Ogloza, W., & Zakrzewski, B. 2004, IBVS, 5507

Pribulla, T., & Rucinski, S. M. 2006, AJ, 131, 2986

Qian, S. 2001a, MNRAS, 328, 635

Qian, S. 2001b, MNRAS, 328, 914

Qian, S. 2002, A&A, 384, 908

Qian, S. 2003, A&A, 400, 649

Qian, S. B., & Zhu, L. Y. 2002, ApJ, 568, 1004

Qian, S.-B., et al. 2013a, ApJS, 209, 13

Qian, S.-B., et al. 2014, ApJS, 212, 4

Qian, S.-B., et al. 2017a, ApJ, 848, 131

Qian, S.-B., He, J.-J., Zhang, J., Zhu, L.-Y., Shi, X.-D., Zhao, E.-G., & Zhou, X. 2017b, Res. Astron. Astrophys., 17, 087

Qian, S.-B., Liu, N.-P., Liao, W.-P., He, J.-J., Liu, L., Zhu, L.-Y., Wang, J.-J., & Zhao, E.-G. 2013b, AJ, 146, 38

Qian, S.-B., Zhang, J., He, J.-J., Zhu, L.-Y., Zhao, E.-G., Shi, X.-D., Zhou, X., & Han, Z.-T. 2018, ApJS, 235, 5

Qian, S.-B., Zhu, L.-Y., & Boonruksar, S. 2005, New Astron., 11, 52

Rahunen, T. 1981, A&A, 102, 81

Rovithis-Livaniou, H., Kranidiotis, A. N., Rovithis, P., & Athanassiades, G. 2000, A&A, 354, 904

Rucinski, S. M., Pribulla, T., & van Kerkwijk, M. H. 2007, 134, 2353

Russo, G., Vittone, A. A., & Milano, L. 1984, A&AS, 57, 69

Samec, R. G., Flaaten, D., Jaso, A., Oliver, B., & Rehn, T. 2012, PASP, 124, 1025

Smith, R. C. 1984, QJRAS, 25, 405

Stepien, K., & Gazeas, K. 2012, Acta Astron., 62, 153

Terrell, D., & Wilson, R. E. 2005, Ap&SS, 296, 221

Tian, X.-M., Zhu, L.-Y., Qian, S.-B., Li, L.-J., & Jiang, L.-Q. 2018, Res. Astron. Astrophys., 18, 020

Van Hamme, W. 1993, AJ, 106, 2096

Van Hamme, W., & Wilson, R. E. 2007, ApJ, 661, 1129

Vilhu, O. 1981, Ap&SS, 78, 401

Vilhu, O. 1982, A&A, 109, 17

Wang, J.-J., Jiang, L.-Q., Zhang, B., Zhao, S.-Q., & Yu, J. 2017, PASP, 129, 124202

Wilson, R. E. 1990, ApJ, 356, 613

Wilson, R. E. 1994, PASP, 106, 921

Wilson, R. E. 2012, AJ, 144, 73

Wilson, R. E., & Devinney, E. J. 1971, ApJ, 166, 605

Yang, Y.-G., Dai, J.-M., Yin, X.-G., & Xiang, F.-Y. 2007, AJ, 134, 179

Yang, Y.-G., Lü, G.-L., Yin, X.-G., Zhu, C.-H., & Nakajima, K. 2009a, AJ, 137, 236

Yang, Y.-G., Wei, J.-Y., & Nakajima, K. 2009b, PASJ, 61, 13

Zhang, Y., Han, Q.-W., & Liu, J.-Z. 2016, PASP, 128, 124201